PRENTICE-HALL SERIES

Roberts and Vanderslice



Ultrahigh Vacuum and its Applications

# ULTRAHIGH VACUUM

## AND ITS APPLICATIONS

### Richard W. Roberts

General Electric Research Laboratory

### Thomas A. Vanderslice

Vacuum Products, General Electric

PRENTICE-HALL, INC.

Englewood Cliffs, N.J.

#### © 1963 by Prentice-Hall, Inc., Englewood Cliffs, N.J.

All rights reserved. No part of this book may be reproduced in any form, by mimeograph or any other means, without permission in writing from the publisher.

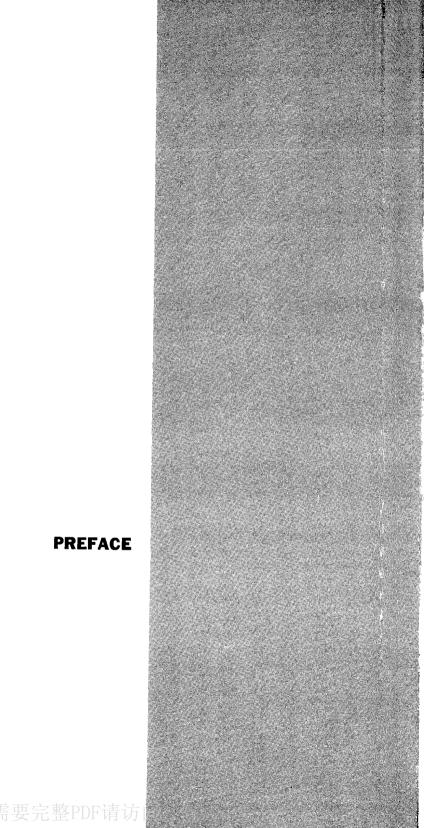
Current printing (last digit):

12 11 10 9 8 7 6 5 4 3

Library of Congress Catalog Card No. 63-18110 Printed in the United States of America C 93565

12

Dedicated to Katharine B. Blodgett and W. D. Walters



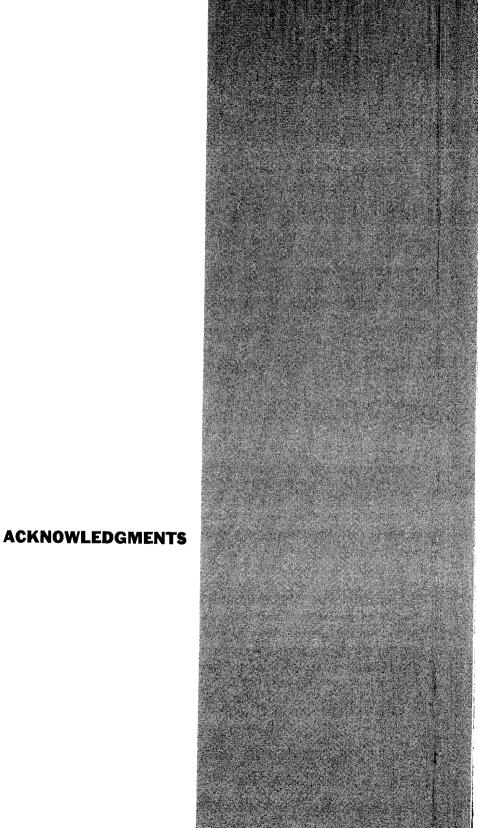
Historically, vacuum technology has been of major importance in the evolution of electronics ever since the first vacuum tube was constructed. Means for obtaining and measuring vacuums have proven indispensable in the development of nearly all electronic devices. Likewise, such means are basic to the understanding of surface physics and surface chemistry.

For many experiments and purposes, pressures of the order of  $10^{-6}$  torr ( $10^{-6}$  mm Hg or about  $10^{-9}$  atmosphere) are low enough, even though surface phenomena studies show that at  $10^{-6}$  torr a surface becomes covered with adsorbed gas in only a few seconds. Other experiments, however, require the use of ultrahigh vacuum. At lower pressures the number of collisions of gas phase atoms and molecules with a surface is so small that a clean surface remains free of contamination long enough to do experiments on the surface itself. Recent surface studies have required pressures of  $10^{-9}$  torr or lower. At this pressure no significant surface contamination occurs for a several-hour period. Pressures of  $10^{-8}$  torr and below are generally called the ultrahigh vacuum range. Ultrahigh vacuum is a requisite for many experiments that involve either the reaction between a surface and a gas or the properties of the surface itself.

Currently, the understanding and application of techniques of ultrahigh vacuum are somewhat restricted to specialists who of necessity are familiar with meeting reports, subject literature that appears in scientific journals, and parts of textbooks. From this material these men have gained a working knowledge of the inherently simple techniques needed in ultrahigh vacuum experiments. It has been clear for some time that a book devoted to the study of ultrahigh vacuum was needed. We trust that this book answers such a need.

Ultrahigh Vacuum and Its Applications is written primarily for the experimental scientist, engineer, or technician who has a nodding acquaint-ance with ordinary vacuum techniques and wishes to extend his knowledge to include ultrahigh vacuum technology. We have carefully considered the components, their theories of operation, their assembly and use, and the nature of the materials of construction necessary for work in this field. Data and guides for the production and use of ultrahigh vacuum have been collected in one place. The impact of ultrahigh vacuum on problems of technology is illustrated by a brief discussion of thin films, catalysis, boundary lubrication, and space simulation. This book spells out how to do it and where to find it.

R. W. Roberts and T. A. Vanderslice



The need for a small book on ultrahigh vacuum technology was first pointed out to us by Dr. F. J. Norton and Dr. L. E. St. Pierre. Dr. St. Pierre participated in the early preparation of the manuscript and wrote the section on boundary lubrication (7-2).

We are grateful to Dr. K. B. Blodgett and Dr. G. L. Gaines, Jr., for their penetrating criticisms of the manuscript and their many suggestions for improvement. We would also like to thank Dr. P. Cannon, Dr. C. W. Tucker, Dr. N. R. Whetten, and Dr. J. R. Young for helpful discussions.

Mrs. N. L. Gaertner and Miss C. W. Wilson aided in the preparation of the figures and tables.

# 1

#### Ultrahigh Vacuum Technology

- 1-1 Introduction, 2
- 1-2 The History of Ultrahigh Vacuum Technology, 5

# 2

#### **Ultrahigh Vacuum Components**

- 2-1 Introduction, 8
- 2-2 Fundamental Vacuum System Considerations, 8
- 2-3 Pumps for Ultrahigh Vacuum, 10
- 2-4 Gauges for Ultrahigh Vacuum Measurement, 30
- 2-5 Bakeable Gauges for Pressures  $> 10^{-5}$  Torr, 50
- 2-6 Valves for Ultrahigh Vacuum, 58
- 2-7 Accessories for Ultrahigh Vacuum, 62

# 3

### **Material of Construction**

- 3-1 Introduction, 84
- 3-2 Glass, 95
- 3-3 Ceramic Refractory Materials, 105
- 3-4 Metals, 109

# 4

## Ultrahigh Vacuum Systems

- 4-1 Introduction, 122
- 4-2 Assembly, 122
- 4-3 Typical Systems, 125
- 4-4 Leak Detection, 130
- 4-5 Operation, 131

# 5

#### Generation of Clean Surfaces

- 5-1 Introduction, 136
- 5-2 Evaporation, 137
- 5-3 High Temperature Heating of Bulk Metal, 142
- 5-4 Ion Bombardment (Sputtering), 143
- 5-5 Cleaving of Single Crystals, 144
- 5-6 Field Desorption, 145

# 6

## **Physical Properties of Surfaces**

- 6-1 Introduction, 148
- 6-2 Thermionic and Field Emission from Surfaces, 148
- 6-3 Field Emission and Field Ion Microscopes, 153
- 6-4 Low Energy Electron Diffraction, 157
- 6-5 Electron Emission by Ions and Electrons, 161
- 6-6 Flash Filament Experiments, 165

# 7

## Miscellaneous Applications

- 7-1 Physical and Chemical Properties of Thin Films, 174
- 7-2 Boundary Lubrication of Metals,177
- 7-3 Space Simulation, 179

## **Appendix—General References**

- A Ultrahigh Vacuum References, 186
- B General Vacuum References, 186
- C Journals, 187

#### Index

- A Name Index, 189
- B Subject Index, 193

Table 2-1. Evapor-ion pumping speeds, p.19.

Table 2-2. Classification of metals and semi-metals based on adsorption properties, p.27.

Table 2-3. Ionization gauge sensitivity ratios r for various gases, p.35.

Table 2-4. High pressure data for the Bayard-Alpert ionization gauge, p.56.

Table 2-5. Sensitivity and range of high-pressure ionization gauge, p.57.

Table 2-6. List of low-melting-point alloys suitable for use as liquid-metal, high vacuum seals, p.68.

Table 2-7. Impurities observed upon introducing helium into vacuum system by three different methods, p.74.

Table 3-1(a-c). Vapor pressure data and melting and boiling points for the more common elements, pp.85-87.

Table 3-2. Vapor pressure data for a number of common gases, p.91.

Table 3-3. Composition of the more common Corning glass, p.97.

Table 3-4. General features of the permeation of gases through glasses, metals, and semiconductors, p.99.

Table 3-5. Diffusion constants and solubilities for helium and a number of glasses, p.101.

## **TABLES**

Table 3-6. Permeation constants for a variety of gases and Vycor glass or fused silica, p.101.

Table 3-7. Comparison of tungsten and lanthanum boride as electron sources for ionization gauges, p.104.

Table 3-8. Temperatures (°C) at which stability no longer exists in surface-to-surface contact of some refractory materials in vacuum, p.108.

Table 3-9. Relative degrees of reaction between materials at 1800°C in an inert atmosphere, p.108.

Table 3-10. Percentage composition of gas evolving from different materials, p.112.

Table 3-11. Spot welding of various metal combinations, p.113.

Table 3-12. Typical materials and temperatures used to make reactive alloy seals, p.118.

Table 5-1. Techniques and refractory support materials for evaporating metals together with some useful vapor pressure data, pp.138-141.

Table 6-1. Work functions changes for nitrogen on tungsten, p.152.

Table 6-2. Secondary electron emission properties of elements and compounds, pp.171-173.

Fig. 1-1. A plot of the log of the surface coverage time as a function of the log of the pressure, p.4.

Fig. 2-1. Three-stage mercury diffusion pump, p.11.

Fig. 2-3. Fractionating oil diffusion pump, p.12.

Fig. 2-4. Molecular sieve trap, p.12.

Fig. 2-5. Copper foil trap, p.13.

Fig. 2.6. Simplified energy diagram for the adsorption of a diatomic gas on a metal surface, p.14.

Fig. 2-7. Modified Bayard-Alpert ionization gauge, p.15.

Fig. 2-8. Change in number of atoms in gas phase with time in an ionization gauge, p.16.

Fig. 2-9. Temperature dependence of recovery rate for argon, p.17.

Fig. 2-10. Cleanup of argon vs. voltage on collector cylinder, p.18.

Fig. 2-11. Evapor-ion pump, p.20.

Fig. 2-12. Titanium ion pump system, p.20.

Fig. 2-13. Penning ionization gauge, p.21.

Fig. 2-14. Varian ion pump, p.22.

Fig. 2-15. Autoradiograph of Kr<sup>85</sup> in the cathode of a commercial ion pump, p.23.

Fig. 2-16. Pattern of pressure vs. time for a getter-ion pump exhibiting argon instability, p.24.

Fig. 2-17. Third electrode ion pump, p.24.

Fig. 2-18. Cross-section view of a slotted cathode ion pump, p.25.

Fig. 2-19. Cathode of a diode ion pump after pumping benzene at pressures of  $10^{-5}$  torr, p.26.

## **FIGURES**

Fig. 2-20. Titanium getter pumped vacuum system, p.28.

Fig. 2-21. Liquid helium cryogenic pump, p.31.

Fig. 2-22. Useful ranges of vacuum gauges, p.31.

Fig. 2-23. Probability of ionization as a function of electron energy, p.32.

Fig. 2-24. Bayard-Alpert ionization gauge, p.32.

Fig. 2-25. Conventional ionization gauge compared with a Bayard-Alpert ionization gauge, p.32.

Fig. 2-26(a,b). Collector current vs. grid voltage for a Bayard-Alpert and a conventional ionization gauge, p.34.

Fig. 2-27. Hot-cathode magnetron ionization gauge, p.36.

Fig. 2-28. Hot-cathode Penning ionization gauge, p.36.

Fig. 2-29. Hot-cathode magnetron ionization gauge, p.37.

Fig. 2-30. Ionization gauge with a photomultiplier electron source, p.38.

Fig. 2-31. Calibration of the photomultiplier electron source ionization gauge vs. a Bayard-Alpert gauge, p.38.

Fig. 2-32. Cold-cathode magnetron ionization gauge, p.39.

Fig. 2-33. Inverted cold-cathode magnetron ionization gauge, p.39.

Fig. 2-34. Magnetic deflection mass spectrometer, p.42.

Fig. 2-35. Schematic diagram of the magnetic deflection mass spectrometer shown in Fig. 2-34, p.42.

Fig. 2-36. Mass spectra of the isotopes of carbon monoxide, p.43.

Fig. 2-37. Recording of a mass spectrum of CO and  $N_2$  isotopes for a total pressure of  $1.4 \times 10^{-11}$  torr, p.44.

Fig. 2-38. Physical arrangement of the experimental time-of-flight mass spectrometer, p.45.

Fig. 2-39. Simplified omegatron mass spectrometer, p.46.

Fig. 2-40. Schematic diagram of the Bennet type of radio frequency mass spectrometer, p.47.

Fig. 2-41. Cutaway diagram of a twenty-gap linear radio frequency mass spectrometer, p.49.

Fig. 2-42. Schematic drawing of cross-field mass spectrometer, p.49.

Fig. 2-43. Schematic drawing of quadrupole mass filter, p.49.

Fig. 2-44. U-tube manometer, p.50.

Fig. 2-45. Oil manometer for ultrahigh vacuum use, p.50.

Fig. 2-46. Typical McLeod gauge, p.51.

Fig. 2-47. Null-reading manometer, p.52.

Fig. 2-48. Block diagram of null-reading manometer, p.53.

Fig. 2-49. Circuit diagram for the Pirani gauge, p.54.

Fig. 2-50. Circuit diagram for the thermocouple gauge, p.54.

Fig. 2-51. Circuit diagram for the thermistor gauge, p.54.

Fig. 2-52. Normalized ion current vs. pressure curve for argon, p.56.

Fig. 2-53. Normalized ion current vs. pressure curve for helium, p.56.

Fig. 2-54. High pressure ionization gauge with cylindrical geometry, p.57.

Fig. 2-55. High pressure ionization gauge with plane geometry, p.57.

Fig. 2-56. High pressure ionization gauge characteristics for  $N_2$ , He, and  $H_2$ , p.58.

Fig. 2-57. Granville-Phillips bakeable metal valve, p.59.

Fig. 2-58. Bakeable metal valve, p.59.

Fig. 2-59. Seat for metal valve, p.60.

Fig. 2-60. Two types of glass break seals, p.61.

Fig. 2-61. Glass valve, p.61.

Fig. 2-62. Glass valve, p.61.

Fig. 2-63. Liquid metal valve, p.62.

Fig. 2-64. Demountable metal flanges: (a) metal O-ring seal; (b) knife edge seal; (c) step seal; (d) "Conflat" seal, p.63.

Fig. 2-65. Coined metal gasket design, p.64.

Fig. 2-66. Flexible bellows, p.65.

Fig. 2-67. Crystal cleaving apparatus for measuring gas content of crystals, p.66.

Fig. 2-68. Rotary motion seal, p.66.

Fig. 2-69. Rotary motion seal using a low vapor pressure liquid seal, p.67.

Fig. 2-70. Bakeable rotary seal, p.68.

Fig. 2-71. Vacuum system for evaporating ultrapure nickel films and measuring their magnetic properties, p.69.

Fig. 2-72. Disk-type glass-metal molecular pump, p.70.

Fig. 2-73. Metal Diffusion leaf for admitting gases to vacuum systems, p.72.

Fig. 2-74. Metal-ceramic leak, p.73.

Fig. 2-75. Porcelain leak, p.73.

Fig. 2-76. Bakeable microbalance, p.75.

Figs. 3-1(a-c). Vapor pressure data for the more common elements, pp.88-90.

Figs. 3-2(a,b). Vapor pressure data for the more common gases, p.92.

Fig. 3-3. Coefficient of linear expansion of many of the more common metals and alloys, p.93.

Fig. 3-4. Coefficient of linear expansion for Corning glasses, p.94.

Fig. 3-5. Coefficient of linear expansion for several ceramic materials, p.95.

Fig. 3-6. Volume-temperature curve for a glass forming system, p.96.

Fig. 3-7. Viscosity-temperature curves for several Corning glasses, p.98.

Fig. 3-8. Permeation rate of helium through a number of different glasses, p.100.

Fig. 3-9. Atmospheric gas accumulation in a silica bulb, p.103.

Fig. 3-10. Helium accumulation from the atmosphere in bulbs of different glasses, p.103.

Fig. 3-11. Lime glass to Pyrex graded seal, p.105.

Fig. 3-12. Microstructure of a commercial ferrite, p.105.

Fig. 3-13. Microstructure of a typical porcelain, p.106.

Fig. 3-14. Electrical resistivity of several refractory oxides as a function of temperature, p.107.

Fig. 3-15. Permeability of metals to gases, p.110.

Fig. 3-16. Housekeeper glass-to-metal seal, p.116.

Fig. 3-17. Housekeeper seal joining a hard and soft glass, p.116.

Fig. 3-18. Photograph of ceramic tubes, p.118.

Fig. 3-19. Mica-to-metal bakeable seal, p.119.

Fig. 4-1. Schematic diagram of general ultrahigh vacuum system, p.123.

- Fig. 4-2. Over-all view of a typical laboratory ultrahigh vacuum system, p.124.
- Fig. 4-3. A commercially available ultrahigh vacuum pump station, p.125.
- Fig. 4-4. Schematic diagram of an ultrahigh vacuum system used for the study of gas-metal film reactions, system I, p.126.
- Fig. 4-5. Schematic diagram of a versatile ultrahigh vacuum system for studying gas-metal film reactions, system II, p.128.
- Fig. 4-6. Photograph of the ultrahigh vacuum system shown schematically in Fig. 4-5, p.128.
- Fig. 4-7. Schematic diagram of a metal ultrahigh vacuum system, system III, p.129.
- Fig. 5-1. Evaporation sources, p.137.
- Fig. 6-1. Potential-energy diagram for electrons in a metal, p.149.
- Fig. 6-2. Work functions of many of the elements, p.150.
- Fig. 6-3. Charge distribution at a metal surface, p.151.
- Fig. 6-4. The change in work function of a polycrystalline tungsten surface as a function of coverage by cesium, p.151.
- Fig. 6-5. Potential-energy diagram for electrons as a metal surface in the presence of an applied field without an image potential, p.152.
- Fig. 6-6. Schematic diagram of a field emission microscope, p.153.
- Fig. 6-7. Field emission pattern from a clean tungsten tip, p.154.
- Fig. 6-8 (a-c). Field emission patterns for barium on tungsten, p.155.
- Fig. 6-9. Helium ion image of a tungsten tip, p.156.

- Fig. 6-10. Schematic diagram of a lowenergy electron diffraction tube using a movable Faraday cage detector, p. 158.
- Fig. 6-11. Schematic diagram of a lowenergy electron diffraction tube using postacceleration of the diffracted electrons, p.158.
- Fig. 6-12. Schematic diagram of a lowenergy electron diffraction tube using magnetic deflection of the incident and diffracted electrons and postacceleration of the diffracted electrons, p.159.
- Fig. 6-13 (a-c). Typical low-energy electron diffraction patterns obtained from a clean platinum crystal, p.160.
- Fig. 6-14. Low-energy electron diffraction pattern obtained from the (111) face of platinum after heating to 365°C in oxygen and then cooled in oxygen, p. 160.
- Fig. 6-15. Electronic transitions involved in the so-called direct process of potential ejection illustrated for He<sup>+</sup> on Mo, p.161.
- Fig. 6-16. Schematic views of an instrument designed for the study of electron ejection by ion impact, p.162.
- Fig. 6-17. Yield  $\gamma_i$  of electrons ejected by He<sup>+</sup> ions from tungsten in various surface conditions during cleaning by heating, p.163.
- Fig. 6-18. Kinetic energy distributions,  $No(E_k)$ , of electrons ejected by 40-eV He<sup>+</sup> ions from tungsten, p.164.
- Fig. 6-19. Schematic diagram of a flash filament apparatus, p.166.
- Fig. 6-20. Sticking probabilities for a number of gases on tungsten (the 411 plane) at room temperature as a function of surface coverage, p.167.

Fig. 6-21. Desorption spectra of nitrogen from a tungsten wire initially at 100°K, p.167.

Fig. 7-1. The effect of oxygen pressure during film preparation on the magnetic characteristics of a tin film, p.175. Fig. 7-2. Rate of decomposition of

ethane on a 27°C rhodium surface and the rate of product formation, p.177.

Fig. 7-3. Schematic diagram showing the generation of clean metal during a wear process, p.178.

Fig. 7-4. Atmospheric pressure given as a function of altitude (height above the earth), p.180.

Fig. 7-5. Vapor pressure of the common gases at low temperatures, p.182.

Fig. 7-6. Schematic diagram of the cryogenic wall of a space simulator, p.183.

Fig. 7-7. Schematic diagram of the General Electric M.S.V.D. space simulator, p.183.